Available online at www.sciencedirect.com
SCIENCE DIRECT®
ELSEVIER
International Journal of Solids and Structures 42 (2005) 3867–3896
INTERNATIONAL JOURNAL OF SOLIDS and STRUCTURES
www.elsevier.com/locate/ijsolstr

A continuum constitutive model for the mechanical behavior of woven fabrics

M.J. King *, P. Jearanaisilawong, S. Socrate

Department of Mechanical Engineering, Massachusetts Institute of Technology, Cambridge, MA 02139, USA

Received 8 June 2004; received in revised form 20 October 2004
Available online 21 January 2005

Abstract

We propose a new approach for developing continuum models for the mechanical behavior of woven fabrics in planar deformation. We generate a physically motivated continuum model that can both simulate existing fabrics and predict the behavior of novel fabrics based on the properties of the yarns and the weave. The approach relies on the selection of a geometric model for the fabric weave, coupled with constitutive models for the yarn behaviors. The fabric structural configuration is related to the macroscopic deformation through an energy minimization method, and is used to calculate the internal forces carried by the yarn families. The macroscopic stresses are determined from the internal forces using equilibrium arguments. Using this approach, we develop a model for plain weave ballistic fabrics, such as Kevlar®, based on a pin-joined beam geometry. We implement this model into the finite element code ABAQUS and simulate fabrics under different modes of deformation. We present comparisons between model predictions and experimental findings for quasi-static modes of in-plane loading.

Keywords: Woven fabric; Continuum modeling; Kevlar

1. Background

The mechanical behavior of woven fabrics is of interest in numerous applications, including apparel, fabric reinforced composites, and body armor for ballistic protection. A number of current research efforts are focused on the integration of woven fabrics with other technologies such as flexible electronics, microfluidics, or ''actuated'' materials (such as synthetic muscle fibers) to obtain hybrid woven systems with advanced capabilities. Examples include body armor with embedded medical sensors or communications

* Corresponding author. Tel.: +1 617 324 0164; fax: +1 617 324 1553.
E-mail address: mking@mit.edu (M.J. King).

0020-7683/$ - see front matter © 2004 Elsevier Ltd. All rights reserved.
doi:10.1016/j.ijsolstr.2004.10.030

equipment, apparel with microfluidic cooling or heating capabilities, or clothing that augments the physical capabilities of the wearer. Development of these technologies requires a thorough understanding of the mechanical behavior of woven fabrics.

The mechanical behavior of even relatively simple plain-weave fabrics is complex due to the intricate interactions of the yarns that constitute the fabric "mesostructure". Despite many attempts to develop effective models for fabric behavior, there is currently no widely accepted modeling approach that can accurately capture all of the important aspects of fabric deformation and effectively predict both the macroscopic mechanical response of the fabric as well as the response of the component yarns at the mesostructural level. This is due in part to the variability of requirements for fabric models in different applications. Specialized fabric models employing various approaches have been proposed by researchers from several industries. A number of these models are summarized below.

One of the simplest approaches used to model fabrics is to homogenize the behavior of the underlying mesostructure and approximate the fabric as an anisotropic continuum. In the framework of a continuum formulation, a woven fabric can be treated as an anisotropic planar continuum with two preferred material directions. Homogenized formulations for fabrics or fabric composite structures have been proposed by a number of different researchers. These include Steigmann (1992) and Baseau (2003), who have developed continuum formulations for "filamentary networks" appropriate for non-reinforced fabrics, Reese (2003), who considers an elastoplastic anisotropic continuum formulation, Xue et al. (2003) and Shockey et al. (1999a,b, 2001, 2002a,b), who describe continuum models for woven composites, and Raun and Chou (1995) and Gommers et al. (1996) who use continuum models for knitted composites.

Continuum models typically allow greater computational efficiency and are easily integrated into multi-component system models. However, the identification of appropriate homogenized material parameters can be a formidable challenge. Different researchers have approached this challenge in different manners. For example, Xue et al. determine material properties through empirical testing, while Shockey et al. rely both on empirical testing and on detailed finite element modeling. Reese employs mixed element modeling of the fabric mesostructure to determine the constitutive properties for a continuum model.

Unfortunately, most traditional continuum models proposed in the literature do not account for the effect of interactions between the yarn families. These interactions include:

- *crimp interchange*, a mechanism by which the fabric elongates along the direction of one yarn family with negligible yarn stretching, as the yarns of that family become less crimped (i.e. the yarn waves decrease in amplitude and increase in wavelength), while the fabric contracts along the direction of the other yarn family, as the yarns of that family become more crimped;
- *locking*, a mechanism by which the fabric resists deformations as the interwoven yarns jam against each other;
- *resistance to relative yarn rotation*, which is the dominant mechanism for the response of fabric to in-plane shear. These are important behaviors in many fabric applications. The omission of potentially important behaviors makes traditional continuum models unsuitable for the general analysis of novel fabric systems where both the macroscopic behavior at the continuum level and the yarn interactions at the mesostructural level may be important.

A large number of mesostructurally based analytical models have been developed for the study of these behaviors. Mesostructurally based analytical models use mathematical relations to predict the mechanical response of the fabric and its component yarns in specific modes of deformation. For example, a model could be formulated to predict the load–extension behavior of a fabric under uniaxial or biaxial tension along the warp or weft yarn family directions. Mesostructural models can be used to quantify homogenized material properties for use in continuum models. Hearle et al. (1969) describe a number of classical analytical fabric models. One of the most widely adopted of these, a model proposed by Peirce (1937), shown in

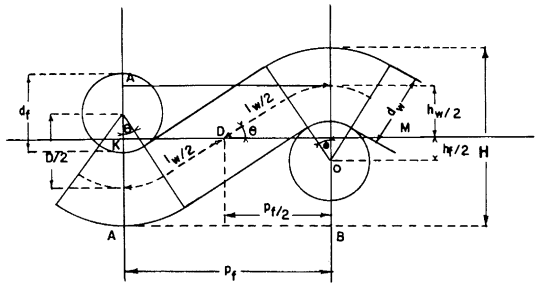

Fig. 1. Geometry proposed by Peirce (1937).

Fig. 1, provides a mathematical framework for relating the parameters that describe the geometrical configuration of a plain weave fabric with circular yarns.

A number of researchers have employed modified forms of Peirce's geometry to account for yarns with non-circular deformable cross sections. Warren (1992) uses such a modified geometry to predict the low-load response to uniaxial and biaxial tension along the yarn families of a plain woven fabric based on elastic beam theory with coupled yarn extension and bending effects. Sagar et al. (2003) also employ a modified form of this geometry and use the principle of stationary potential energy to determine the fabric configuration and deformation in response to an applied load. However, all such analytical models are only valid in the specific loading modes for which they have been developed; for example, both Warren's and Sagar's models assume that the yarn families remain orthogonal and hence neither of these models allows shear deformation. Extension of these models to more general load cases is challenging due to the complexity of their geometry.

Because Peirce's geometry is fairly detailed, other researchers have proposed simpler models in order to achieve greater mathematical simplicity or computational efficiency. In a series of classical articles, Kawabata et al. (1973a,b,c) propose analytical models for the biaxial, uniaxial, and shear deformation behaviors of fabrics based on the much simpler pin-joined truss geometry shown in Fig. 2. Other researchers have subsequently employed this geometry to develop improved analytical models, including Realff et al. (1997) who modify Kawabata's uniaxial model to include more complex behaviors such as yarn flattening and consolidation. Kato et al. (1999) propose an analytical model for predicting the constitutive behavior of a coated fabric composite that is based on the pin-joined lattice-type geometry shown in Fig. 3. This geometry is similar to that proposed by Kawabata but with additional spars to capture the effect of the

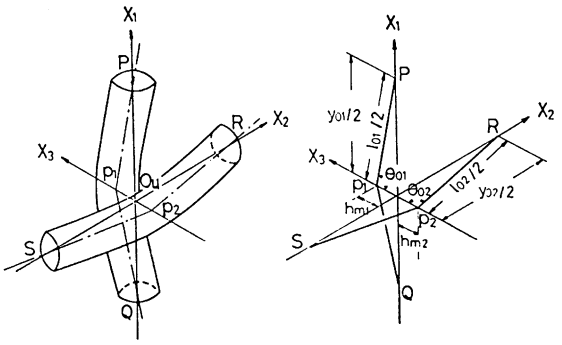

Fig. 2. Geometry proposed by Kawabata et al. (1973a).

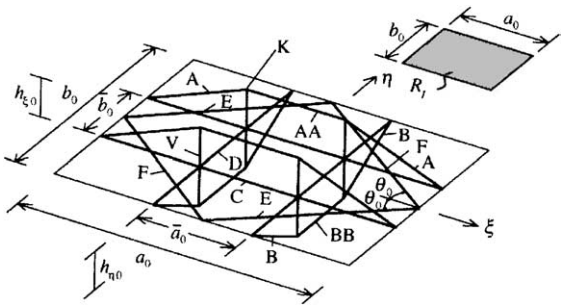

Fig. 3. Fabric lattice geometry used by Kato et al. (1999).

coatings and create a unit cell capable of resisting shear deformation. A detailed summary of several other analytical fabric models is given by Realff (1992).

Analytical models of the fabric mesostructure can be incorporated into anisotropic continuum formulations to yield models that track the fabric mesostructure as the continuum deforms, thereby combining the benefits of continuum modeling with the capability of following the evolution of the fabric mesostructure in a single modeling step. Boisse and his colleagues (1997, 2001) have developed a four-node finite element for simulating the response of plain weave fabric composites during forming processes. The yarn directions evolve as the elements deform and the yarn-direction behaviors are based on Kawabata's analytical model, thereby allowing accurate prediction of biaxial fabric behavior with evolving material directions. Rattensperger et al. (2003) take a similar approach for modeling fabric-reinforced hydraulic hoses, with fabric lattice geometry similar to that used by Kato, and use a conventional finite element formulation with rebar reinforcements. However, neither Boisse's nor Rattensperger's models include yarn bending effects, locking, or resistance of the fabric to shear. On the other hand, Tanov and Brueggert (2003) present a mesostructurally based continuum model that includes shear and locking resistance through diagonal spar elements within the assumed unit cell network, but Tanov's model does not include crimp interchange. No sufficiently general mesostructurally based continuum model has yet been proposed.

An alternate approach to capture the mechanical response of woven fabrics is to abandon continuum modeling and use numerical modeling to directly capture the fabric mesostructure. One approach is to directly model every yarn in the fabric as shown in Fig. 4. This method, used by Ng et al. (1998), Boisse et al. (2001), and Shockey et al. (1999a,b, 2001, 2002a,b) among others, has the advantage of capturing all yarn interactions and providing a detailed description of all mechanisms of fabric deformation.

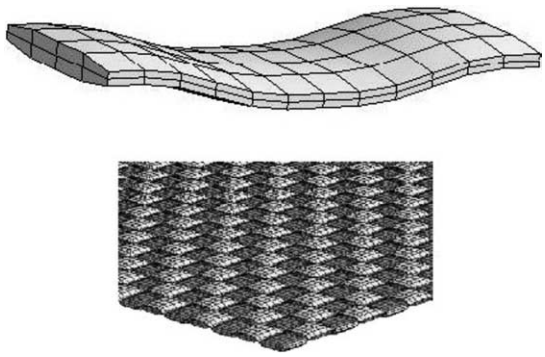

Fig. 4. Shockey's detailed FE model of a plain weave reinforcing fabric (Shockey et al., 1999a).

However, its very large computational requirements limit it to relatively small systems. This approach is not suitable to the analysis of large or multicomponent systems, and is generally used only to gain insight into the mechanics of fabric deformation at the mesostructural level, to estimate homogenized properties for simpler continuum models, or to characterize the interactions of the yarns. Furthermore, the constitutive behavior of the individual yarns can be a source of model uncertainty, as the yarns themselves are generally not homogeneous but rather are composed of individual fibers; describing this complex morphology may require even more detailed sub-modeling. In order to achieve greater computational efficiency, a mix of simpler, more efficient finite elements (such as beams or spars) can be used to directly model the entire fabric mesostructure. A wide variety of models have employed this mixed element approach, including the model proposed by Reese (2003), the model proposed by MacGlockton et al. (2003), which uses a mixture of truss and solid elements to model 3D textile composites, and the model proposed by Cherouat and Billouet (2001) for pre-impregnated woven composites, which uses truss elements and membrane elements.

Other researchers have used alternative techniques that do not rely on a finite element discretization, especially for ballistic analyses. The most widely used model for predicting the ballistic response of fabrics was proposed by Roylance et al. (1995) and consists of a planar rectangular array of point masses to capture the inertia of the fabric, connected by trusses to capture the yarn compliances. Extensions and improvements to this model have been proposed by a number of researchers, including Shim et al. (1995), and have been shown to be effective in specialized cases at predicting the ballistic performance of certain classes of woven fabrics. However, models of this type capture only selected aspects of the behavior of the fabric mesostructure and therefore are not suitable for more general analyses. A completely different approach has been proposed by Breen et al. (1994), who use a model composed of interacting particles to predict the low stress behavior, especially draping, of woven fabrics.

These existing approaches to fabric modeling tend to be specialized. A more universal modeling approach that can be tailored to a wide variety of different applications is required for the development of advanced fabric systems. Such an approach would also be useful in the analysis of existing fabric applications. In this paper, we propose a general approach for the systematic development of a mesostructurally-based continuum model for the mechanical behavior of woven fabrics. This approach has the following properties:

- It relates the behavior of the fabric on the macroscopic scale, as characterized by the macroscopic deformation gradient, loads, and stresses, to the response of the fabric's mesostructure, as characterized by the geometrical configuration of the weave and the loads acting on the yarns. However, unlike many established mixed-mode or homogenization approaches (which generally require multiple modeling steps at different length scales), this approach integrates the two relevant length scales into a single model.
- It is sufficiently general to simulate the known responses of a fabric as well as to predict the behavior of a novel fabric based on the measured properties of the component yarns and yarn interactions.
- It can be tailored to a variety of different applications by selecting appropriate geometrical and constitutive assumptions. While the resulting model will, of course, be specialized to the specific application, the same modeling method can be used to develop models for a wide variety of purposes.

2. Model development

2.1. Mechanics of an anisotropic planar continuum

In a continuum description, yarns are not modeled explicitly; rather, the woven fabric is treated as a homogenized anisotropic material, as shown in Fig. 5. The characteristic length scale for the boundary

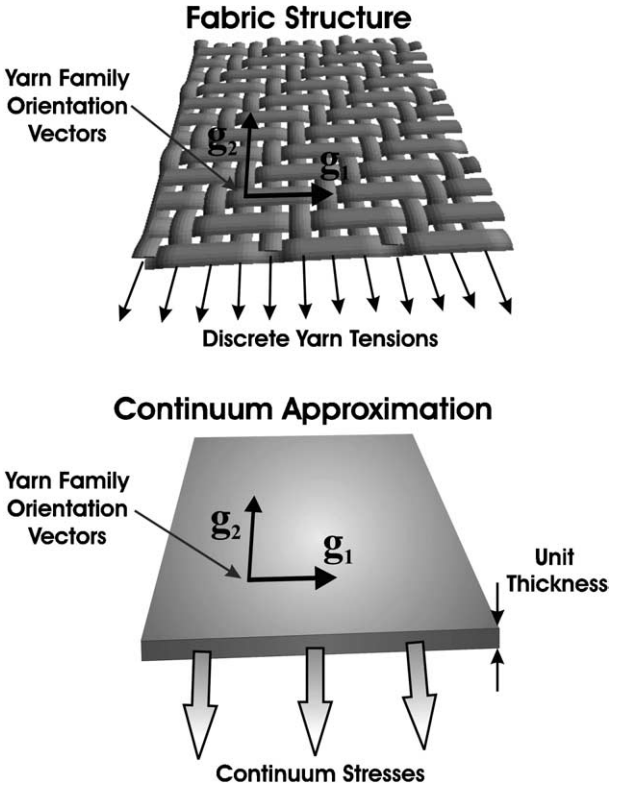

Fig. 5. Approximating a fabric as an anisotropic continuum.

value problem to be treated with this approach must be sufficiently large compared to the length scale of the fabric mesostructure. Two families of vectors can be used to describe the orientation and deformation of the yarn families at each continuum material point. The deformed configuration of the individual yarns must be related to the macroscopic state of deformation and the loads carried by individual yarns must be related to the macroscopic state of stress.

The macroscopic state of deformation is typically described using the deformation gradient, designated by $\mathbf{F}$, where components in a Cartesian coordinate systems are obtained as:

$$F_{jk}(t) = \frac{\mathrm{d}x_j(t)}{\mathrm{d}X_k}. \tag{1}$$

Here $x_j(t)$ is the i-coordinate of a material point at time t, and X_k is the i-coordinate of that point in the undeformed configuration. The deformation gradient $\mathbf{F}$ describes the transformation of material lines with deformation: a vector ${}^{0}\mathbf{a}$ that describes a material line in the undeformed configuration is transformed by deformation into a vector $\mathbf{a}$ according to:

$$\mathbf{a} = \mathbf{F}{}^{0}\mathbf{a}. \tag{2}$$

The deformed length a of this vector is given by:

$$a = \sqrt{\mathbf{a}\cdot\mathbf{a}} = \sqrt{(\mathbf{F}{}^{0}\mathbf{a})\cdot(\mathbf{F}{}^{0}\mathbf{a})} = \sqrt{{}^{0}\mathbf{a}\cdot(\mathbf{F}^{\mathrm{T}}\mathbf{F}){}^{0}\mathbf{a}}. \tag{3}$$

The angle θ between two material lines **a** and **b** can be determined from the dot product of the two:

$$\mathbf{a} \cdot \mathbf{b} = (\mathbf{F}^{\mathbf{0}}\mathbf{a}) \cdot (\mathbf{F}^{\mathbf{0}}\mathbf{b}) = ab\cos\theta. \tag{4}$$

These relations imply that if the deformation gradient at a point is known, the deformed length, orientation, and angles between material lines at that point can be calculated.

The "true" stress measure in the loaded (deformed) configuration is the Cauchy stress, $\boldsymbol{\sigma}$. If a small surface with area $\mathrm{d}S$ within the deformed body is defined by a vector $\mathbf{n}\mathrm{d}S$, where **n** is the unit normal to the surface, and the Cauchy stress in the body at that point is $\boldsymbol{\sigma}$, the traction force vector **t** that results from $\boldsymbol{\sigma}$ acting on $\mathrm{d}S$ is given by:

$$\mathbf{t} = \boldsymbol{\sigma}\mathbf{n}\,\mathrm{d}S. \tag{5}$$

This is the macroscopic stress measure that must be determined from the applied deformation history in order to define a continuum constitutive model.

Many of the challenging aspects of modeling fabric behavior, such as capturing crimp interchange and locking, relate to the in-plane response of the fabric. Furthermore, with the exception of three-dimensional weaves, the out-of-plane behavior of a fabric is typically only weakly coupled to the in-plane behavior in the absence of out-of-plane loads. (Large out-of-plane loads, such as transverse shear stresses or through-thickness compression, will obviously have a significant effect on the in-plane response of the fabric). In this paper, we introduce a two-dimensional planar model that captures only the in-plane response of the fabric. This model cannot be used to predict out-of-plane displacements or bending, transverse shear responses, or changes to the fabric thickness. We are currently working to extend the model to a three dimensional implementation using a shell formulation, where the membrane fabric behavior will be captured using the approach developed here for the planar behavior. For the current planar model, the relevant stresses and strains are the in-plane normal components $\{\sigma_{11}, \sigma_{22}\}$ and $\{\varepsilon_{11}, \varepsilon_{22}\}$ and the in-plane shear components σ_{12} and ε_{12}. The out-of-plane response is considered decoupled from the in-plane response and the through-thickness strain resulting from in-plane extension and contraction is neglected. No external out-of-plane loadings are considered. Under these conditions, plane stress and plane strain conditions are equivalent, as σ_{33} and ε_{33} are both identically zero. The choice of the out-of-plane model dimension is arbitrary and so, for simplicity, a constant unit thickness is assumed for the fabric continuum.

2.2. General approach and limiting assumptions

We adopt a number of limiting assumptions to simplify our model. The current model is intended for quasi-static analysis of fabrics subjected only to in-plane loads. It does not include failure mechanisms such as yarn breakage, unraveling of the weave, and yarn pullout. For deformation histories where these failure modes are not present, yarn slip at the crossover points will be negligible. We rely on the assumption that no yarn slip occurs (i.e., the yarns act as if they were pinned together where they cross). This assumption implies that the crossover points deform in an affine manner with the fabric continuum and the vectors describing the yarn family orientations and wavelengths are material lines. Such a "slip-free" model is accurate until the onset of failure, when yarn slip begins to dominate the response of the fabric. We are currently developing more advanced continuum fabric models that include the effects of yarn slip.

The fabric configuration, yarn loads, and macroscopic stresses can be determined from the state of macroscopic deformation through the following five steps:

1. Select a geometry that represents the fabric and define a unit cell (Section 2.3).
2. Associate constitutive relations with the interactions and deformations of the yarns within the unit cell (Section 2.4).

3. Establish a method for determining the geometric configuration of the fabric mesostructure from the macroscopic deformation gradient (Section 2.5).
4. Calculate loads carried by the yarns in the deformed fabric configuration (Section 2.6).
5. Transform these mesostructural loads into continuum stresses at the macroscopic scale (Section 2.6).

This approach is sufficiently general to permit the development of models appropriate for a wide variety of applications. The geometry and constitutive relations chosen in the first two steps control which behaviors a model can capture and determine its computational efficiency and accuracy; hence these choices can be used to tailor the model to a specific application.

In order to demonstrate the application of this approach, we have used it to develop a model for the in-plane, quasi-static behavior of a ballistic fabric, Kevlar® S706, manufactured by DuPont. Kevlar® S706 is a plain weave fabric composed of multifiber untwisted yarns. While our current model is concerned only with capturing the in-plane, quasi-static behavior of this fabric, we plan to expand it to a three-dimensional, dynamic implementation suitable for simulating ballistic impacts. Consequently, we include all in-plane behaviors that affect the fabric's ballistic response. During a ballistic impact the material at the point of impact is displaced out of the plane of the fabric and the resulting elongation of the fabric around the impact zone causes strains and stresses to develop along the impacted yarns. These strains and stresses propagate along yarns away from the impact zone more quickly than the out-of-plane displacement wave. The strains increase until yarns fail as the projectile penetrates the fabric. Yarns not directly impacted are affected because they are interwoven with yarns that are affected. For a detailed description of the phenomena that occur during ballistic impact, see Cunniff (1992).

Due to the large velocities involved in the process and the fact that the fabric's in-plane stiffness is much larger than its bending stiffness, out-of-plane inertial effects and in-plane stiffness effects dominate the fabric ballistic response. In-plane shear is important as it affects the inward flow of material, although shear angles typically remain small-to-moderate ($<30°$) before failure occurs. Locking may be important as it can arrest the inward flow of material, and crimp interchange is important since it directly affects the in-plane stiffness and the propagation of the strain wave fronts. Resistance to yarn bending has only a small effect on the response of the fabric due to the extremely small bending stiffness of the yarns; however, these effects stabilize the low-stress fabric response. All these aspects of the in-plane fabric behavior (locking, shear deformation, crimp interchange, yarn bending) have been included in the current implementation of the quasi-static planar model.

2.3. Geometry

We have adopted a geometry similar to that proposed by Kawabata (1973), as shown in Fig. 6. The yarns are represented as a network of trusses connected by pin-joints at their crossover points. These trusses do not lie in the plane of the fabric but are interwoven to capture crimp interchange. They have axial compliance to allow for yarn stretch but are infinitely stiff in bending. The effects of yarn bending are modeled as being concentrated at the crossover points, where bending is resisted by rotational "bending springs". Interactions between yarns at the crossover points are captured by "crossover springs" connecting the pin joints. The crossover springs have two modes of deformation. They are capable of extending and contracting to simulate the effects of cross-sectional deformation, allowing the yarns to change their crimp amplitude while remaining in contact. The spring elements also offer elastic and dissipative resistance to relative in-plane rotation of the yarn families—the mechanisms for in-plane fabric shear. Similar truss networks have been used by a number of different authors, such as Ben Boubaker et al. (2002), to represent fabric weave geometries.

This geometric representation is somewhat simplistic. Its chief limitation is that it models the yarns as straight with sharp corners at the crossover points, whereas the yarns actually wrap around the crossing

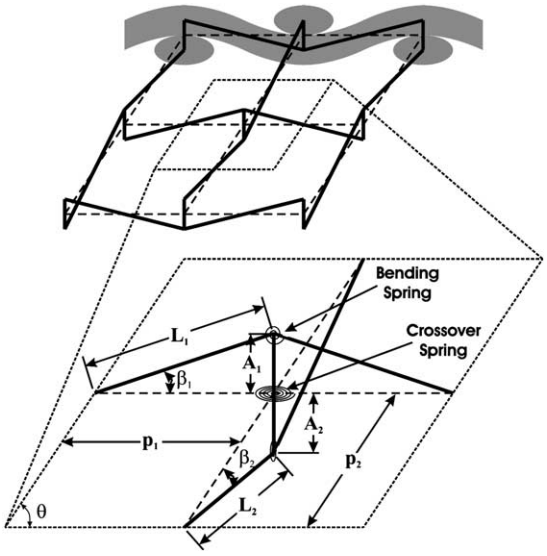

Fig. 6. Kevlar® fabric model geometry.

yarns with a smooth radius of curvature. This geometry consequently permits configurations that are incompatible because of interpenetrations between the yarns, and cannot capture complex behaviors that are controlled by yarn wrapping. However, the effects of wrapping become significant only in very tight weaves with solid yarns, or at very high shear angles. For the specific Kevlar® fabrics and load cases considered in this work, where the yarns are composed of multiple fibers and the shear angles are typically small-to-moderate, wrapping effects are not expected to impact the fabric response significantly. The proposed geometric description therefore is adequate for capturing the relevant behaviors and is more computationally efficient than more sophisticated geometric descriptions. This modeling approach can be extended to other applications by selecting more suitable geometric descriptions capable of capturing behaviors relevant to those applications.

Kevlar® fabrics exhibit locking behavior, where yarns of one family jam against yarns of the other family either due to large shear deformations (''shear locking'') or to crimp interchange (''cross locking''), as shown in Fig. 7. During locking, the yarn cross-sections deform as the yarns are compressed against one another. The model geometry does not track changes in the size or shape of the yarn cross sections; however, locking effects can be accounted for by introducing truss elements that remain normal to the yarns, as shown in Fig. 8. These locking trusses simulate contact forces between the yarns and resist further deformations when locking conditions are met.

The configuration of the unit cell geometry is described by the parameters shown in Figs. 6 and 8:

- the quarter-wavelengths p_i,
- the half yarn lengths between crossover points (yarn length per quarter-wavelength, hereafter referred to simply as ''yarn lengths'') L_i,
- the crimp angles β_i,
- the crimp amplitudes A_i,
- the locking truss lengths d_i,
- the inclination α_i of the locking trusses to the fabric plane, and
- the in-plane included angle between the yarn families θ.

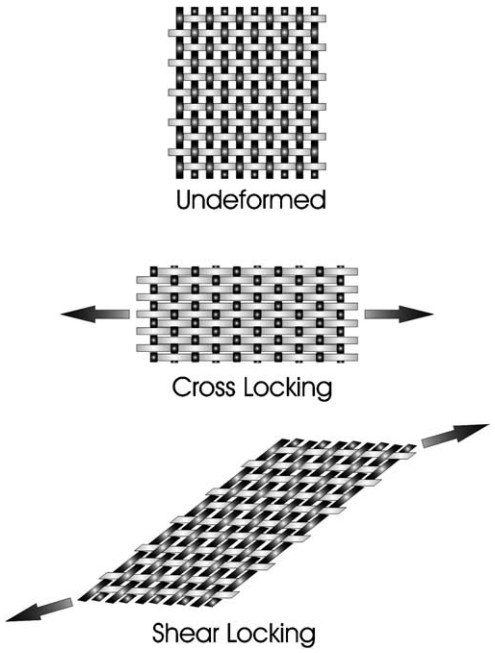

Fig. 7. Cross locking (from crimp interchange) and shear locking (from shear deformation) in a plain weave.

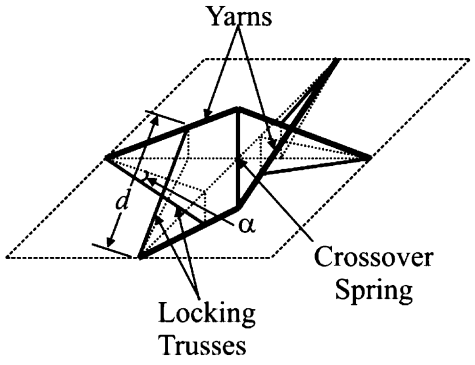

Fig. 8. Locking trusses normal to the yarns.

We have adopted the convention that the subscript "i" designates the yarn family—1 for the warp yarns and 2 for the weft yarns. Several of these parameters are related through geometric constraints, so that of the thirteen parameters listed, only five are independent. For example, in the selected geometry, amplitude and crimp angle can be related to wavelength and yarn length through the following expressions:

$$A_i = \sqrt{L_i^2 - p_i^2}, \tag{6}$$

$$\cos\beta_i = \frac{p_i}{L_i}. \tag{7}$$

Only the two wavelengths, the two yarn lengths, and the angle of relative yarn rotation are required to completely describe the geometrical configuration of the unit cell.

2.4. Component constitutive relations

Constitutive relations provide a means of calculating the forces carried by the components of the unit cell and the energy stored (or dissipated) when the fabric is deformed into a certain configuration. A constitutive relation is required for every mode of energy storage or dissipation in the model: eight are necessary for the planar Kevlar® fabric model proposed here. Four describe the response to extension and the bending of the two yarn families. One describes the response to interference between the warp and weft yarns at the crossover points and one describes the response to interference that occurs during locking. The seventh and the eighth relations describe the elastic and the dissipative responses as the yarns rotate relative to each other at the crossover points to accommodate in-plane shear.

Once fully extended, Kevlar® yarns generally exhibit linear elastic behavior. Therefore, the model uses linear elastic relations to describe yarn extension from an initial length ${}^0L_i$ to a deformed length L_i:

$$T_i = k_i(L_i - {}^0L_i), \tag{8}$$

where T_i is the tensile force in the yarns of the ith family and k_i is the stiffness of the yarn segments in the unit cell (which may differ between the two yarn families). Some sources (Shim et al., 1995; Shim et al., 2001) suggest that Kevlar® may display rate dependent behavior at large strain rates ($>100\,s^{-1}$). While not considered in the present implementation, rate dependence of yarn extension could be readily included in the model. Our current model is for quasi-static analysis, where Kevlar® is effectively rate-insensitive.

Within the high-stress deformation regime, the energy associated with yarn bending is small compared to that associated with yarn extension. However, under certain boundary conditions (where the fabric is free to deform along one yarn family), bending resistance is the dominant resistance to deformation (other than inertia) before the onset of locking or the point where the loaded yarns straighten. Therefore, yarn bending resistance must be included in order to guarantee a non-zero stiffness at low strains for all admissible sets of boundary conditions. For the selected geometry, bending is modeled as concentrated at the pin joints corresponding to the crossover points. Bending resistance is imparted through rotational springs at these points and is assumed to be linear elastic, with the bending moment M_{bi} exerted on the yarns at the crossover points proportional to the change in the crimp angle β_i:

$$M_{bi} = k_{bi}(\beta_i - {}^0\beta_i). \tag{9}$$

If necessary, the "initial" crimp angle ${}^0\beta_i$ can be adjusted to account for different amounts of permanent set in the yarns.

Relations describing interactions between yarns at the crossover points are generally difficult both to measure and to model at the macroscopic level, since they involve interactions between yarn fibers at a very small scale. In general, the magnitude of the deformations of the yarn cross-sections is a non-linear function of the force between yarns and possibly other parameters, such as the relative diameters and angles of the crossing yarns or the tensions carried by the yarns. The proposed model adopts a significant simplification: the effects of cross sectional deformations at the crossover points are captured by a non-linear "interference spring". This spring simulates soft contact conditions, with negligible stiffness in tension and an initially compliant compressive response that becomes increasingly stiff as the interference increases. An exponential relation with two material parameters K_I and a has been chosen to capture this behavior:

$$F_I = K_I(e^{aI} - 1). \tag{10}$$

Here I is the interference between the cross-sections of the crossing yarns and is defined as the sum of the initial crimp amplitudes (one half of the fabric thickness) minus the sum of the current crimp amplitudes.

This interference relation is fairly simplistic. A number of researchers, such as Chen et al. (2001) and Realff (1992, 1997), have shown that yarn interactions at the crossover points are more accurately described by far more complex relations. They have proposed models to capture these interactions that include additional dependencies such as yarn tension or represent the interactions through distributed pressures rather than point loads. More sophisticated relations would allow more accurate predictions of the fabric thickness and of the fabric response to transverse pressure loads. However, the effects of these more sophisticated relations on the in-plane response of the fabric to in-plane loads are expected to be small. Since the current model is intended only for planar analysis, Eq. (10) is used in the interest of computational efficiency.

When the fabric locks, the yarns jam against each other and their cross sections are forced deform in order to avoid interference. During locking, the ovalized yarns in Kevlar® S706 typically deform along their longer cross-sectional axis (parallel to the fabric plane), as opposed to the shorter axis (through the fabric thickness), which is aligned parallel to the interference spring. Consequently, the locking response will be more compliant than the response of the crossover-point interference spring. A power law relation is used to describe the compressive force F_L that develops in the locking trusses when their length has been shortened by an amount I_L:

$$F_L = \begin{cases} 0 & I_L \leqslant 0 \\ K_{\mathrm{d}}(I_L)^c & 0 < I_L \end{cases}, \tag{11}$$

with $I_L = d_0 - d$, where d is the length of the locking truss and d_0, the length of the truss when locking would first start to occur, depends on the geometry of the yarns and weave. The locking trusses have no stiffness in tension. The coefficient K_{d} and the exponent c are two material parameters that, together with the parameters describing the initial geometry, determine the locking behavior. More sophisticated models for yarn interactions during locking can be implemented should this relation prove unable to faithfully capture the fabric response.

In-plane shear is accommodated by relative rotation of the yarn families at the crossover points, known as "trellising". A large number of works concerning the experimentally measured shear response of woven materials appear in the literature: for example, the works of Mohammed et al. (2000) and Peng et al. (2004). Fabrics typically can exhibit three regimes of shear behavior, shown schematically in Fig. 9.

A very stiff elastic response is followed by a compliant response where yarns begin to rotate, resisted primarily by friction. For many fabrics, the initial elastic portion of the response is negligible. As rotation angles become larger, stiffening due to locking or wrapping effects is evident. Finally, the fabric locks and

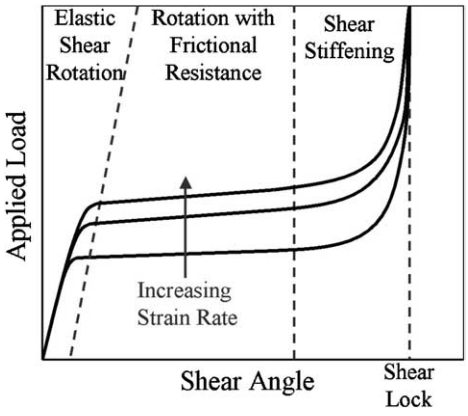

Fig. 9. Typical fabric behavior in shear.

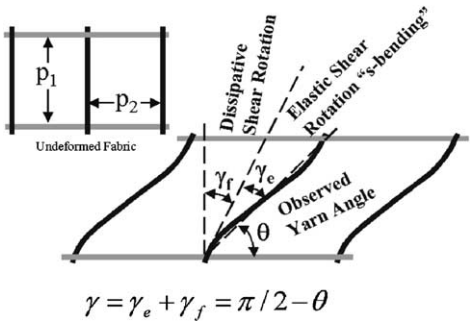

Fig. 10. Weave schematic (top view) showing decomposition of the relative yarn rotation angle.

stresses become very large, and more complex mechanisms of deformation (such as unraveling or wrinkling) occur. Stiffening and locking are captured through the locking trusses. The portion of the shear response that does not originate from locking can be additively decomposed into an elastic portion that results from ''s-shaped'' bending between the crossover points and a dissipative portion that results from rotation of the yarns at the crossover points, as shown in Fig. 10.

Very little purely elastic shear occurs prior to the onset of dissipative rotation, and experiments indicate that the shear response over this small elastic region is approximately linear:

$$M = K_s \gamma_e. \tag{12}$$

The elastic stiffness K_s is large enough so that dissipative rotation initiates at very small shear angles (on the order of 10^{-2} rad). A rate-dependent power law is used to represent the dissipative component of the yarn rotation, with $\dot{\gamma}_0$ giving the reference dissipative rotation rate at a reference moment M_0, and an exponent b capturing the rate sensitivity of the dissipative shear behavior:

$$\dot{\gamma}_f = \dot{\gamma}_0 \left(\frac{M}{M_0} \right)^b. \tag{13}$$

The parameters in this expression may exhibit dependencies on the fabric state (e.g., frictional resistance to rotation may be greater when the contact forces between yarns are higher). In the current model implementation, these parameters are considered as constant material properties.

2.5. Determining the fabric configuration

The geometric and constitutive relations characterize the behavior of the fabric mesostructure, but in a continuum model the mesostructural behavior must be related to the behavior of the macroscopic continuum. A means of determining the fabric mesostructural configuration from the macroscopic deformation gradient is required. For the selected geometry, five independent parameters are required to characterize the fabric configuration at a given location. A convenient set consists of the quarter wavelengths p_i, the yarn lengths L_i, and the angle between yarn families θ. More complicated geometries, especially those used to represent different weave patterns (e.g. twill or satin weaves) would require more independent parameters.

At the continuum level, the yarn families can be described by vectors aligned with the yarns, with magnitudes equal to the quarter wavelengths. Under the assumption that no slippage occurs at the crossover points, the crossover points deform in an affine manner with the continuum and hence these vectors are material lines. The quarter wavelengths and the angle between the yarn families can be determined directly from the deformation gradient using Eqs. (3) and (4).

The deformation gradient does not directly determine the other independent parameters required to characterize the fabric configuration. With only the wavelengths p_i and yarn angle θ fixed, an infinite number of configurations are possible with varying yarn lengths L_i of the two families, controlling the balance between the energy stored in yarn extension and yarn bending in each of the two families and the energy stored in the interference spring at the crossover points. Each configuration corresponds to a particular level of elastic energy stored within the unit cell. Energy based arguments can therefore be used to determine the preferred fabric configuration.

At a given instant of time, when the macroscopic state of deformation and the instantaneous amount of dissipative deformation are known, the fabric will assume the configuration with the smallest stored elastic energy. In the current model, with only two free parameters, the energy at a specific time can be visualized as a conditional function of the two yarn lengths, as shown in Fig. 11.

This ''conditional energy function'' will depend on the deformation gradient and the value of any state variables in the model (i.e., for the current model the dissipative shear rotation angle γ_f). The values of the free parameters L_1 and L_2 can be found by minimizing the conditional energy function with respect to these parameters while holding constant state variables and geometrical parameters determined by the deformation gradient. In most cases, numerical techniques are necessary to minimize the conditional energy function, as a closed form for the state of minimum energy does not exist.

More complicated representative geometries (e.g. geometries used to represent other weave patterns, such as twill and satin weaves) will have a larger number of free parameters. The conditional energy functions associated with some geometries may not even have a single global minimum. Multiple minima would correspond to multiple stable states that the fabric structure could assume at a given state of macroscopic deformation. In these cases, the choice of an appropriate numeric minimization scheme is critical, because the efficiency of the minimization scheme depends on the number of free parameters, and also because some schemes converge to the local minimum nearest to the initial guess, while others converge to the global minimum. At this time we have not considered in detail any geometry other than the one shown in Fig. 6, which always has a single global minimum.

2.6. Determining the internal forces and macroscopic stresses

Once the fabric configuration is determined, the internal forces acting on the fabric mesostructural components, including yarn tensions, yarn bending moments, moments between yarns, and contact forces, can be calculated from the component constitutive relations. These internal forces must be transformed into equivalent macroscopic continuum stresses.

For simple hyperelastic fabric models where the fabric configuration can be calculated exactly, the macroscopic state of stress can be calculated by differentiating the complete strain energy function (as opposed

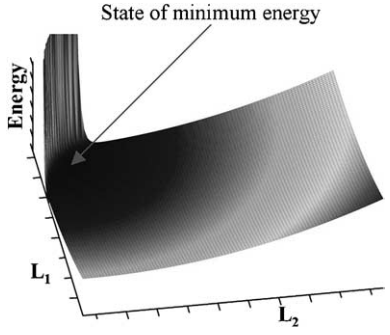

Fig. 11. Conditional energy as a function of L_1 and L_2 at a given deformation gradient.

to the conditional energy function used to determine the fabric configuration) with respect to a tensor describing the deformation. Unfortunately, this approach is not applicable for cases where the strain energy function cannot be expressed in closed form. This is the case for the proposed model because the fabric configuration must be determined numerically. Therefore, the stress must be related to the internal forces using equilibrium arguments. Applying the Cauchy stress to the faces of the deformed unit cell, using Eq. (5), must result in traction forces on each face that balance the internal forces acting on that face. Such a stress tensor can be derived by the following procedure:

1. Determine all load-bearing mesostructural members that are "cut" by the boundaries of the unit cell.
2. Determine the forces that these mesostructural members exert on the unit cell faces.
3. Find the components of these forces that lie in the plane of the fabric. (The out-of-plane components should cancel).
4. Resolve the in-plane forces along vectors parallel to the yarn directions, designated by unit vectors $\mathbf{g_i}$.
5. Divide the resolved forces by the appropriate projected areas to obtain stresses. Express the results in tensorial form in terms of the yarn direction vectors $\mathbf{g_i}$.
6. Check to ensure that the resulting stress tensor is symmetric.

The stress tensor for the Kevlar® fabric model has contributions from yarn tensions T_i, yarn bending moments M_{bi}, the locking forces F_{Li}, and the moment between the yarn families M:

$$\begin{aligned}\boldsymbol{\sigma} = {} & \frac{1}{2p_2\sin\theta}\left(T_1\cos\beta_1 - \frac{M_{b1}\sin\beta_1}{L_1} - \frac{M\cos\theta}{2p_1\sin\theta} - \frac{F_{L1}p_1}{d_1} - F_{L2}\left(\frac{p_2^2\cos^2\theta}{p_1 d_2} + \frac{p_2\sin\alpha_2 \mid \cos\theta \mid \sin\beta_1}{L_1}\right)\right)(\mathbf{g_1}\otimes\mathbf{g_1}) \\ & + \frac{1}{2p_1\sin\theta}\left(T_2\cos\beta_2 - \frac{M_{b2}\sin\beta_2}{L_2} - \frac{M\cos\theta}{2p_2\sin\theta} - \frac{F_{L2}p_2}{d_2} - F_{L1}\left(\frac{p_1^2\cos^2\theta}{p_2 d_1} + \frac{p_1\sin\alpha_1 \mid \cos\theta \mid \sin\beta_2}{L_2}\right)\right)(\mathbf{g_2}\otimes\mathbf{g_2}) \\ & + \left(\frac{M}{4p_1p_2\sin^2\theta} + \frac{F_{L1}p_1\cos\theta}{2p_2d_1\sin\theta} + \frac{F_{L2}p_2\cos\theta}{2p_1d_2\sin\theta}\right)(\mathbf{g_1}\otimes\mathbf{g_2} + \mathbf{g_2}\otimes\mathbf{g_1}).\end{aligned} \tag{14}$$

The stress expression does not contain the forces in the crossover spring, since this spring does not intersect the unit cell faces. In addition to the force parameters, the stress expression also contains geometrical parameters that describe the current configuration of the unit cell.

3. Numerical implementation of the model

The Kevlar® fabric model has been implemented into ABAQUS/Standard, an implicit finite element code, through a user-defined material subroutine. The current implementation of the model is limited to in-plane, quasi-static analyses only. Issues related to the numerical implementation of the model are briefly discussed in this section.

3.1. Minimization

The minimization of the conditional energy function that relates the deformation gradient to the fabric mesostructural configuration must be performed numerically. Various numerical minimization schemes have been investigated, including simulated annealing, the multidimensional Newton's method, and the downhill simplex method. For a detailed description of these techniques, refer to the work of Press et al. (1992). Of these techniques, the downhill simplex technique was found to be the most effective for the

current model, partly because it does not require derivatives of the conditional energy function. For different model geometries, other numerical minimization techniques may prove more effective.

3.2. Stability and buckling

Steigmann (1992) and Baseau (2003), and others have shown that an un-reinforced elastic network, like the Kevlar® fabric model, is mathematically guaranteed to be stable only as long as the network is in tension. Even when the fabric continuum is constrained to remain planar, the fabric geometry chosen for the current model is unstable and capable of buckling when placed in compression. For the unit cell geometry considered in the proposed model, two modes of buckling are possible: yarns can bend at the crossover points and rotate out of the fabric plane, increasing their crimp (subsequently referred to as "yarn buckling"); or the yarns can rotate about axes perpendicular to the fabric plane, causing a shearing motion of the fabric (subsequently referred to as "shear buckling"). These buckling modes are shown in Fig. 12, and can lead to instabilities for a quasi-static implicit analysis where the stabilizing effects of inertia are not included.

A related shortcoming of the continuum approach is that it does not contain explicit information about the internal material structure, so inertial effects associated with the relative rigid body motions of meso-structural elements are not automatically accounted for in the mass matrix used in dynamic analyses. The continuum fabric model can track the inertial resistance to accelerations of the centers of mass of the yarns, but not the inertial resistance to relative rotation of the yarn segments.

These issues can be addressed by the explicit addition of inertial resistance to yarn rotation. The change over a time increment in both the in-plane and the out-of-plane rotational velocities of the yarns are divided

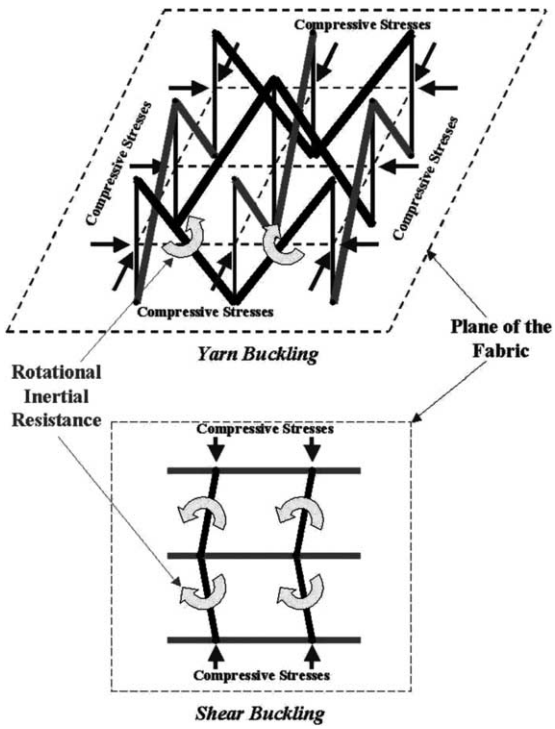

Fig. 12. Buckling modes of the fabric structure, with yarn rotational inertia.

by the length of the time increment to determine average rotational accelerations. The reaction forces and moments corresponding to these rotational accelerations are then be added to the internal unit cell forces. This procedure stabilizes the buckling modes in quasi-static implicit analyses and accounts for the additional rotational inertia of the yarn segments in dynamic analyses.

3.3. Element selection

A finite element discretization cannot predict the exact analytical solution to a general boundary value problem, since the discretization accommodates only a subset of all compatible displacement fields. For most established material models it can be proved that a finite element analysis will predict the displacement field that minimizes the system energy over all displacement fields that it can capture, but this solution will have greater energy than the exact analytical solution. The displacement fields that a given discretization can capture, and hence the accuracy of the analysis, depend on both the density of the finite element mesh and the type of element used. Because of the non-linearities associated with fabric material behavior, element choice has a significant effect on the response of our fabric model. In the presence of non-uniform strain fields when the deformations of the elements are not completely constrained, some element types exhibit non-physical stress oscillations, as illustrated in Fig. 13, and behave in an artificially stiff manner in the low stress regime where crimp-interchange dominates the fabric response.

This behavior is similar to the so-called element "locking" behavior displayed by some elements when used for the analysis of nearly incompressible solids. However, in this case, the oscillations result from the inability of "standard" (linear and quadratic) finite elements to capture strain fields that vary non-linearly across the element. Due to the non-linear phenomenon of crimp interchange, in a fabric subjected to uniaxial extension along one yarn direction a non-linear relationship exists between the axial strain and the transverse strain corresponding to the minimum energy state. For more general modes of deformation, if the direct strain component aligned with one yarn direction varies linearly in space, the direct strain component aligned with the other yarn direction must vary non-linearly in space in order to minimize energy.

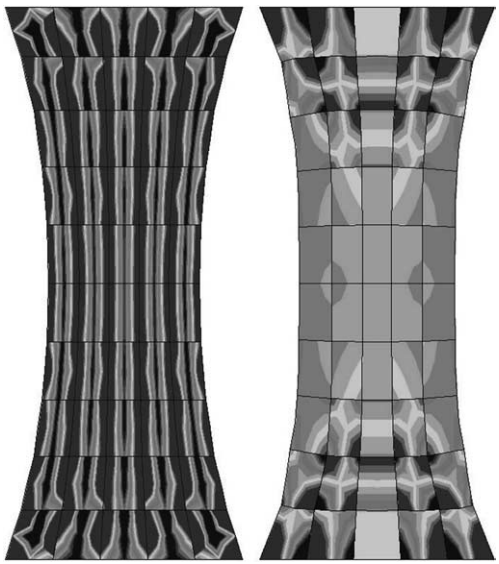

Fig. 13. Stress oscillations in the low-load regime in CPE8 eight-node elements and in CPE8R eight-node reduced integration elements during a simulated tensile test.

Such strain field variations are not attainable with standard elements. The deformation modes with the lowest energies attainable with standard elements exhibit stress oscillations and have a higher energy level when compared to the optimal configuration, even when a very fine mesh is used. Hence, the finite element model will be artificially stiff.

These non-physical stress oscillations can be eliminated by using ABAQUS CPE4R elements, which are four-node linear-interpolation elements with a reduced integration formulation, because in these elements the strain field is sampled only at a single integration point. However, these elements require a very fine mesh for accuracy and also require hourglass stiffness control. Of all the other quadrilateral structural elements available in the finite element code ABAQUS, we have observed that CPE8R elements, which are eight-node quadratic-interpolation elements with a reduced integration formulation, exhibit the smallest stress oscillation amplitudes, with only negligible amounts of associated artificial stiffness. These are the elements we have employed for the analyses presented in this study. After locking or yarn stretching cause significant increases in stress, the stress oscillations become negligible for all element types.

4. Experimental determination of model parameters

The model requires that eleven geometric parameters and thirteen component constitutive properties be defined. In this section we outline experimental techniques that we have used to determine these quantities and present the data obtained for a plain weave ballistic fabric (Kevlar® S706).

The geometric parameters consist of:

- the angles θ_i giving the initial orientations of the yarn families;
- the minor (through-thickness) radii r_i and major (in-plane) radii R_i of the yarn cross-sections;
- the initial quarter wavelengths of the yarn families ${}^0p_i$;
- one of the initial half yarn lengths between crossovers ${}^0L_1$ (the length for the other yarn family ${}^0L_2$ can be calculated from geometric constraints); this parameter determines the initial crimp amplitudes and angles for both yarn families;
- the relaxed crimp angles ${}^0\beta_{\mathrm{i}}$, which reflect the amount of "set" in the bent yarns.

The initial quarter wavelengths and the initial yarn family orientations can be measured directly from a woven fabric sample. The initial half yarn lengths between crossovers (the yarn lengths per quarter-wavelength) and the relaxed crimp angles can be measured from single yarns removed from the weave. These values for Kevlar® S706 are reported in Table 1. The yarn radii cannot be measured in this manner, since they generally change when yarns are removed from the weave.

The shape of the yarn cross-sections in the weave can be determined through microscopy. Fig. 14 shows micrographs of Kevlar® S706 created by embedding unstretched fabric in epoxy, sectioning the sample, and photographing the section under an optical microscope. These section micrographs confirm that the yarns have approximately oval cross sections and that the weft yarn family has greater initial crimp than the warp yarn family, as is indicated by the wavelength and yarn length measurements. However, the yarn radii cannot be accurately measured from these micrographs because of potential variations in the position and orientation of the sectioning plane. The radii, wavelengths, yarn lengths, and amplitudes measured from the micrograph in Fig. 14 are not geometrically consistent with the wavelengths and yarn lengths obtained from macroscopic measurements. A more indirect method of estimating the minor (through-thickness) radii can instead be used. The total thickness of the fabric is measured and apportioned between the two yarn families, as reported in Table 1. The major (in-plane) radii affect only the locking behavior of the fabric, determining the amount of deformation that can occur before the onset of locking (or the initial

Table 1
Measured material parameters for Kevlar® S706

Property	Symbol	Value	Unit
Geometric properties			
Fabric thickness[a]	–	*0.300*	mm
Warp minor (through-thickness) radius	r_1	0.075	mm
Weft minor (through-thickness) radius	r_2	0.075	mm
Warp major (in-plane) radius	R_1	0.400	mm
Weft major (in-plane) radius	R_2	0.400	mm
Initial warp quarter wavelength	${}^0p_1$	0.374	mm
Initial weft quarter wavelength	${}^0p_2$	0.374	mm
Initial warp amplitude[a]	${}^0A_1$	*0.060*	mm
Initial weft amplitude[a]	${}^0A_2$	*0.090*	mm
Initial warp half yarn length between crossovers	${}^0L_1$	0.378	mm
Initial weft half yarn length between crossovers[a]	${}^0L_2$	*0.384*	mm
Warp relaxed crimp angle	${}^0\beta_1$	1.412	Radians
Weft relaxed crimp angle	${}^0\beta_2$	1.334	Radians
Single yarn properties			
Warp yarn stiffness per half yarn length	k_1	3764	N/m
Weft yarn stiffness per half yarn length	k_2	3948	N/m
Warp yarn bending stiffness	k_{b1}	0.00124	N m/rad
Weft yarn bending stiffness	k_{b2}	0.00073	N m/rad
Warp yarn mass density	ρ_1	1441	kg/m^3
Weft yarn mass density	ρ_2	1441	kg/m^3
Interference stiffness properties			
Interference relation coefficient	K_I	0.00309	N
Interference relation exponent	a	1×10^6	1/m
Locking stiffness properties			
Locking stiffness	K_d	1.36×10^{13}	N/m^c
Locking exponent	c	3.70	–
Yarn rotation (shear) properties			
Elastic rotational stiffness	K_s	0.0131	N m/rad
Reference dissipative rotation rate	$\dot{\gamma}_0$	0.00284	Radians/s
Reference dissipative rotation moment	M_0	3.2×10^{-6}	N m
Dissipative rotation rate sensitivity	b	4.0	–

[a] Dependent on other parameters or not required by model.

pre-load of the locking spars in tight, pre-locked weaves). For this reason, these parameters are best obtained by curve-fitting the shear response of the fabric, as described later in this section.

The constitutive parameters that must be defined are:

- the axial stiffnesses k_i of the yarn segments of length L_i;
- the bending stiffnesses of the yarns k_{bi};
- the mass densities of the yarns (for inertial stabilization) ρ_i;
- the two parameters describing exponential interference at the crossover points, K_I and a;
- the two parameters describing the power law locking relation, K_d and c;
- the elastic stiffness associated with relative yarn rotation K_s;
- The two parameters describing rate-dependent dissipative yarn rotation, b and $(\dot{\gamma}_0/M_0^b)$.

The yarn axial and bending stiffnesses can be determined from tension tests performed on single yarns. Fig. 15 shows the results of tests on single weft yarns removed from Kevlar® S706, performed using a

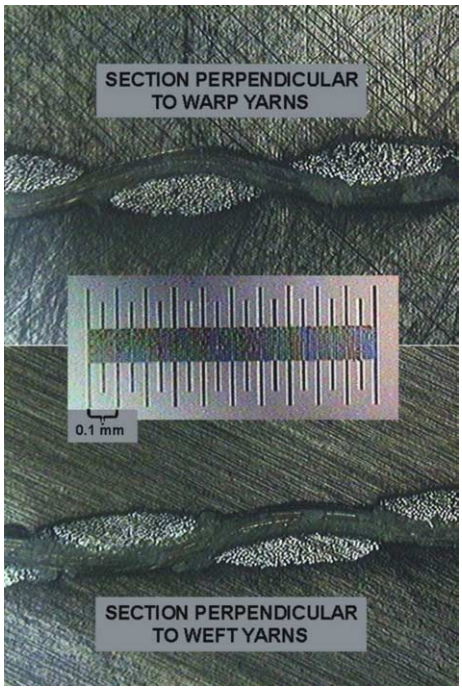

Fig. 14. Micrographs showing cross-sections of Kevlar® S706 woven fabric.

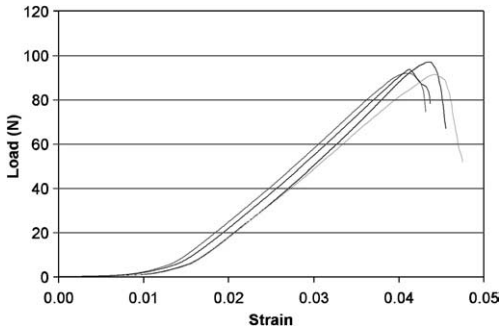

Fig. 15. Load–extension response of single weft yarns removed from Kevlar® S706 fabric.

Zwick tensile tester model BTC-FR010TH.A50. These tests were conducted under quasi-static loading conditions with a strain rate of $0.01\,s^{-1}$.

Because the yarns used in this test had been removed from a woven fabric sample, they were initially crimped rather than straight in the relaxed configuration. Consequently, the load–extension response shows an initially compliant regime as the yarns straighten, followed by a linear elastic response up to a failure load of approximately 90 N. Kevlar® S706 warp yarns behaved in a similar manner but with a shorter compliant response due to lower initial crimp, and a larger average breaking load of approximately 105 N, probably due to the fact that the warp yarns are damaged less during the weaving process. The axial stiffness of the yarns is calculated from the slope of the linear portion of these curves and is reported in Table 1.

The bending stiffness is calculated by manipulating the load–extension data in the uncrimping (low load) regime to obtain the moment acting at the crimp peaks as a function of the crimp angle. These stiffnesses are so small that they have a negligible effect on the response of the fabric in the high-stress regime, but they are sufficiently large to impart non-zero stiffness to the model in the low-stress regime.

The yarn densities are necessary only for inertial stabilization of the buckling modes discussed in Section 3.2 and can be scaled as necessary to improve numerical analysis efficiency, at the cost of increased energy lost artificially to stabilization. We have used the published density for Kevlar®, given in Table 1, which is sufficiently large to attain a stable material response.

The remaining properties, which describe the crossover point interference behavior, the locking behavior, and the yarn rotation behavior, relate to deformation mechanisms that are controlled by interactions between yarns of different families. Consequently, these properties cannot be determined through tests on single yarns. In order to obtain these properties, we conducted tests on samples of woven fabrics and identified the properties by fitting the fabric response in simple, homogeneous modes of deformation. These tests are targeted to identify the specific physical properties relating to the interactions of the yarns. The development of more direct methods to measure or estimate these properties would eliminate the need for fitting the response of the woven fabric.

We investigated the effectiveness of a ''sandwich compression test'', shown schematically in Fig. 16, as a means of determining the properties that govern interference at the crossover points. This test cannot provide a precise measurement of the interference relation properties, as crossover point yarn interference is only one of many competing deformation modes through which the macroscopic deformation in this test can be accommodated. However, this test can provide a useful estimate of the lower bound for the interference properties by assuming that crossover point interference is the only deformation mechanism underlying the macroscopic response. Under this assumption, interference properties obtained by a direct fit of these data are excessively compliant and need to be appropriately scaled. The values selected for the scaled interference properties are given in Table 1. Note that scaling is acceptable because the model shows only a limited dependence of the macroscopic fabric response on the value of these parameters as long as the stiffness of the interference relation is sufficiently large to ensure that interference resistance dominates over bending resistance, thus allowing crimp interchange to occur.

The sandwich test is unsuitable for accurately determining locking properties because it measures resistance to compression along the minor (transverse) axes of the yarn cross-sections, whereas locking results primarily in compression along the major (in-plane) axes. Instead, to obtain these properties we conducted

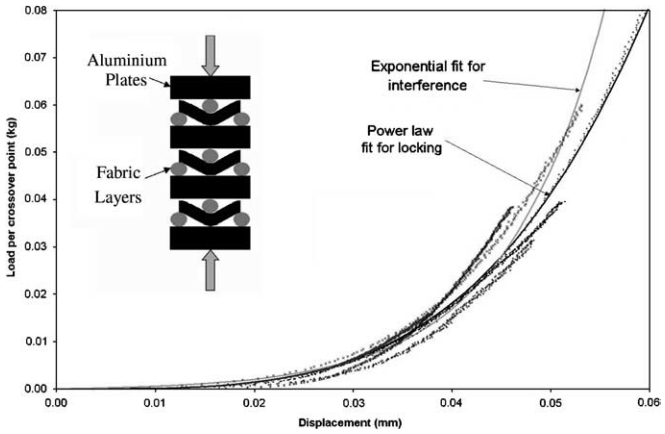

Fig. 16. ''Sandwich'' test to determine interference properties.

so-called ''shear frame'' tests of the type described by McGuinness and O'Bradaigh (1997) and others (e.g., Mohammed et al., 2000; Peng et al., 2004). A shear frame test uses a rhomboidal fixture with hinged corners, as shown in Fig. 17, that grips a square specimen of fabric. Our specimens were 29.0 cm square. Diagonally opposite corners of the shear frame are pulled apart using the Zwick tensile tester. This subjects the fabric to a state of nearly pure yarn rotation, with negligible extension along the yarn directions, until the onset of wrinkling (out-of-plane buckling). This wrinkling was most significant at the corners of the specimen, as they are not subjected to the same shearing loads as the rest of the specimen, and could have been alleviated somewhat by cutting off the corners to make a cruciform-shaped sample. However, in all tests discussed here, the shear frame samples were square, as shown in Fig. 17.

Most of these tests were conducted at an axial displacement rate of 30mm/min, which corresponds to an initial yarn rotation rate of approximately 2.8×10^{-3} rad/s. All of the properties determined from the shear frame tests, except for the rate sensitivity exponent for dissipative yarn rotation, were determined at this rate, which approximately matches the rotation rates in the bias extension tests described in Section 5. Tests at several other rates were performed in order to gain an estimate of the rate sensitivity exponent.

The response to yarn rotation is dominated by resistance to elastic deformation, resistance to dissipative deformation, and by locking. Consequently, the shear frame test is suitable for determining the properties that govern both locking (the yarn major radii R_i and the parameters K_d and c) and yarn rotation (K_s, $\dot{\gamma}_0$, M_0, and b). Fig. 18 shows load–extension responses from the shear frame experiments. After dissipative rotation begins, the shear behavior exhibits an early stiffening response because the S706 fabric is so tightly woven that it is locked in the stress free configuration, and locking forces that try to force the fabric back into an orthogonal configuration must be overcome even at small rotation angles. By simulating the shear frame tests using the model and varying each property in turn, the predicted response can be fitted to the

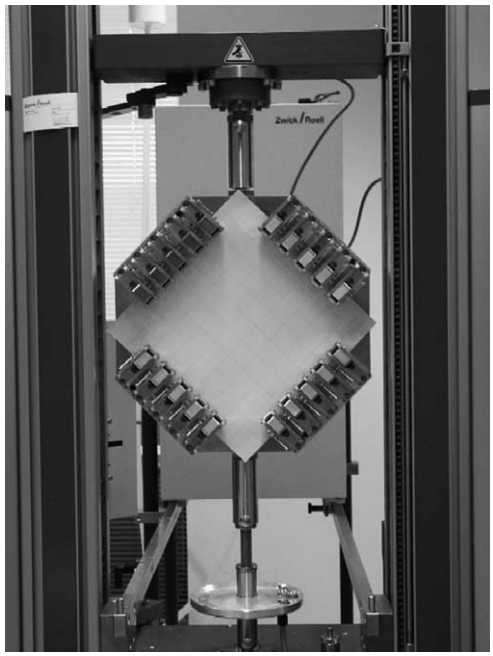

Fig. 17. Shear frame loaded with specimen.

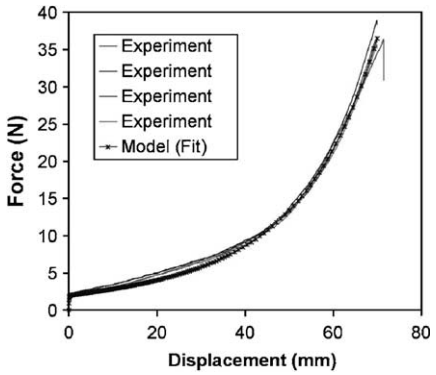

Fig. 18. Model prediction of shear frame behavior with fitted properties, compared to experiments.

experimental data and the locking and yarn rotation properties can be determined. The fitted model response is also shown in Fig. 18, and the corresponding properties are given in Table 1.

5. Comparison of model predictions with experimental findings

5.1. Requirements and description of tests

In order to meet our objectives, the model must be able to:

1. Capture the deformation mechanisms of the fabric and predict, qualitatively and quantitatively, the deformed shape of a fabric specimen under non-homogeneous modes of deformation (Section 5.2).
2. Predict the macroscopic load-displacement response of a fabric specimen (Section 5.3).
3. Predict local mesostructural quantities, such as yarn tensions and contact forces, that pertain to failure mechanisms (Section 5.4).

In order to evaluate these capabilities, we conducted three sets of quasi-static uniaxial tensile tests on strip samples of Kevlar® S706 using the Zwick tensile testing machine. In the first set the load direction was aligned with the warp yarns; in the second set it was aligned with the weft yarns; and in the third set it was oriented at 45° to the yarn directions (“bias-extension”). For the non-bias tests, the load-direction yarns along each edge of the strips were removed over a width of 0.64 cm in order to control the exact number of yarns per specimen and to eliminate effects due to yarn slip and fraying at the free edges, leaving an effective specimen size of 2.54 cm by 25.4 cm with exactly 34 loaded yarns. This large aspect ratio was chosen to minimize end effects at the grips. The bias strips, which undergo much larger elongations before failure, had a smaller initial aspect ratio: 3.5 cm by 9.5 cm. All of the uniaxial strip tests were conducted at $0.01\,s^{-1}$ nominal axial strain rate.

Each of these tests was simulated in ABAQUS/Standard using the geometric parameters and constitutive properties determined in Section 4 and summarized in Table 1. The predictive capabilities of the constitutive model were assessed by comparing the predictions of these simulations to the experimental results. The models were uniformly meshed with approximately square elements of sufficient density as determined through a mesh refinement study. Eight-node reduced integration elements, designated CPE8R elements within ABAQUS, were employed to minimize the mesh-dependent stress oscillations at low load levels, as described in Section 3.3.

5.2. Predicting the macroscopic deformation

The first requirement for the model is the capability to predict the macroscopic deformation of the fabric. In the yarn-direction tensile tests, the fabric strips contract uniformly in the transverse direction along most of their length due to crimp interchange, until the load-direction yarns straighten and crimp interchange ceases. At the grips, where the fabric strip is clamped, no contraction is permitted. This deformation behavior is well predicted by the model, as shown in Fig. 19.

For the warp direction tests, the model predicts that at 4% nominal axial strain, in the region of uniform contraction the fabric strip will have undergone a 4.5% transverse contraction due to crimp interchange, compared to a 4.0% average contraction observed in the experiments. For the weft-direction tests, the model predicts a 5.8% contraction at 4% nominal axial strain, compared to a 5.9% average contraction observed in experiments. Greater contraction occurs in the weft-direction tests because the weft yarns have a greater degree of initial crimp and consequently crimp interchange dominates a larger portion of the response in the weft-direction test.

The simulation predictions of macroscopic deformation patterns are accurate in the bias extension test as well. Fig. 20 shows the predicted and observed deformed shapes and yarn orientations for the bias exten-

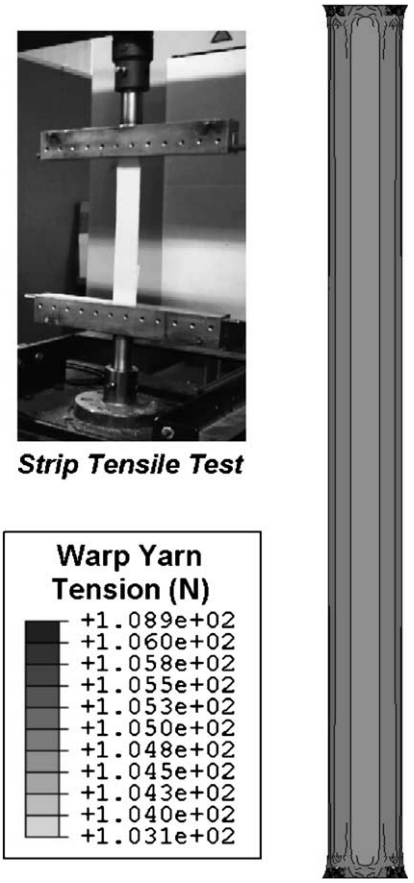

Fig. 19. Warp-direction strip tensile test experiment with deformed shape and warp yarn tensions near failure as predicted by the model (deformation scaled for clarity).

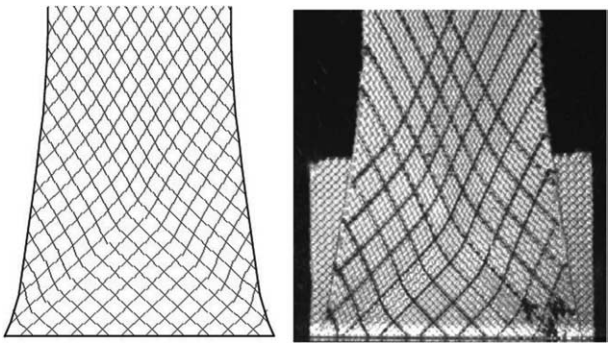

Fig. 20. Predicted and observed deformations and yarn orientations for bias extension test at 17% nominal axial strain.

sion test near the lower grip. The figure on the left shows a vector field describing the yarn orientations at each point. The figure on the right is a photograph of a sample at the same deformation magnitude; the yarn orientations are highlighted by a grid of lines drawn on the fabric parallel to the yarn directions. The simulation predicts the changing yarn orientations very accurately.

In the bias-extension test, the central portion of the strip contracts as the yarns rotate in a trellising manner. As is evident from Fig. 20, the lateral contraction predicted by the simulation and the lateral contraction observed in the experiment are in good agreement. The strip exhibits a triangular low-deformation region at the grip. In the center section of the strip, above these triangular regions, yarn rotation is much greater, as is evident from the sharper yarn angles. The simulation captures these features. Hence there is good agreement between the simulation and the experiments, both in capturing the different regions of deformation and in qualitatively and quantitatively predicting the amount of lateral contraction and the yarn orientations in each region.

5.3. Predicting the macroscopic load–extension response

The second requirement for the model is the capability to predict the macroscopic load–extension response of the fabric. Figs. 21 and 22 show the experimental load–strain curves for the warp and weft direction tests, along with the corresponding model predictions. Note that load has been normalized to average load per yarn; this does not imply that the load carried by all the yarns was the same. The total loads on the samples can be computed by multiplying the loads in Figs. 21 and 22 times the number of yarns in the

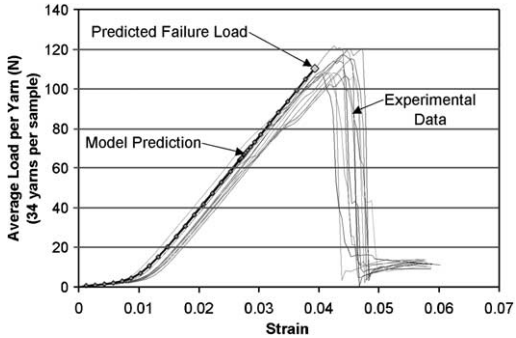

Fig. 21. Model prediction of load–strain behavior in warp direction test compared to experiments.

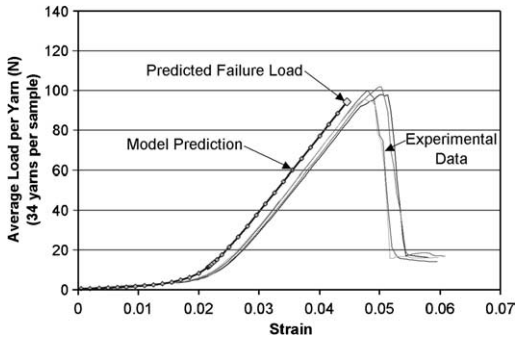

Fig. 22. Model prediction of load–strain behavior in weft direction test compared to experiments.

sample (thirty-four). The model accurately predicts the correct mechanical response using only the properties determined independently from the tests described in Section 4; no curve fitting was performed.

The response in a bias-extension test is dominated by the shear and locking properties of the fabric. Bias tests are generally poorly suited for quantitative comparisons of load responses due to their variability. The extremely low initial resistance to shear deformation combined with the sensitivity of the test to the bias angle and sample orientation results in inconsistency in the experimental measurements. For example, in one set of nine tests, the extension at failure varied between 24 and 32 mm and the failure load varied between 1000 and 1300 N. Therefore, in Fig. 23 we only display experimental load-displacement curves within one standard deviation from the average. Model predictions, obtained using the properties in Table 1, are shown in Fig. 23, together with the experimental results. The model predicts the average bias-extension response accurately with regard to both the strain at which stiffening begins to occur and the stiffened slope.

At larger strains, where the stresses greatly exceed the stresses that develop in the shear frame tests, the model response is too stiff. This may be an effect of the inherent limitations of the current model, which is capable of capturing only failure-free in-plane deformation. The fabric in the bias-extension tests exhibits both wrinkling and unraveling of the weave at large strains, which lead to a more compliant response.

5.4. Predicting the mesostructural response and failure

The last requirement for the model is the capability to predict the response of the fabric at the mesostructural level when the continuum is subjected to macroscopic loading. This is especially important for predicting the onset of failure. The most obvious mode of failure is yarn breakage, which is governed by the tensile

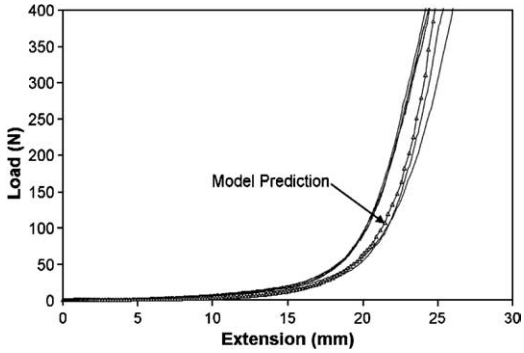

Fig. 23. Selected experimental and predicted load–extension response in the bias-extension test.

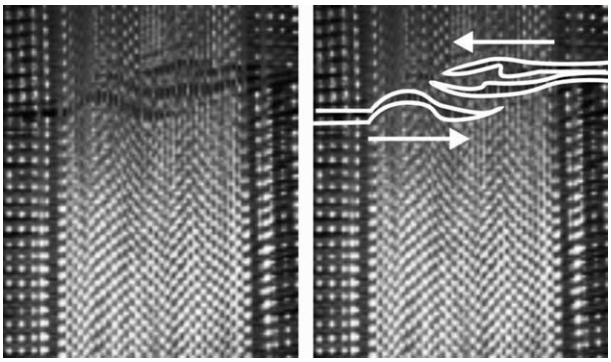

Fig. 24. Failure in a warp-direction tensile test due to yarn breakage, with outer yarns breaking first and failure propagating inwards.

load carried by the yarns. Fig. 19 shows the model predictions for the warp yarn loads in the warp-direction tensile test at 4% nominal axial strain. The model indicates that the outermost yarns carry the greatest loads and therefore will fail first, with yarn failures propagating inwards. This is consistent with the behavior observed during experiments, as shown in Fig. 24.

Furthermore, because the average yarn strengths can be estimated from the single yarn tests, the model can be used to predict the macroscopic loads at which the yarn failure will initiate in the loaded fabric strip, even though the model does not capture failure directly. The data points that lie at the end of the model curves in Figs. 21 and 22 mark the conditions at which the model predicts the onset of failure. The model predictions agree very well with the experimentally observed macroscopic failure loads.

The model can follow the evolution of a wide variety of mesostructural parameters that may be relevant to some other modes of failures or impact the functionality of the woven material, including:

- areal density, which is important when the permeability of the fabric is relevant (e.g., for protection from chemical agents);
- crimp angle, which is relevant if components that are sensitive to bending deformation (such as microelectronics or microfluidics) are woven among the yarn fibers;
- contact forces at the crossover points, which govern the transverse loads on interwoven components and change the resistance to yarn slippage;
- contact forces due to locking, which act as transverse forces on interwoven components and can also cause yarn slippage.

The ability to capture the evolution of such parameters gives the model the flexibility to predict the onset of failure for either a simple fabric or a fabric system with interwoven components.

6. Conclusions and future work

We have proposed a systematic approach for creating fabric continuum models that is sufficiently general to be tailored to a variety of different applications. Continuum models are more computationally efficient and easier to interface with other components of complex structures than discrete models that directly capture individual yarns. Although the continuum models developed using this approach do not directly model individual yarns, they contain information about the behavior of the fabric mesostructure. Through this approach, the response at the fabric mesostructural level to macroscopic loads, and the effects of

mesostructural level innovations on the macroscopic response, can be determined in a computationally efficient manner that is easily integrated with other material models.

The first two steps of the approach rely on development of a representative fabric geometry with a repeating unit cell and of constitutive relations describing the deformations and interactions of the component yarns. These two steps determine the complexity, accuracy, and efficiency of the model. Next, the configuration of the fabric geometry is related to the macroscopic state of deformation of the fabric continuum by minimizing a conditional elastic energy function. Once the fabric configuration is determined from the state of deformation, the internal forces within the fabric unit cell (such as yarn tensions and contact forces) can be calculated from the constitutive relations of the components. Finally, these mesostructural forces are converted into macroscopic continuum stresses. The chief assumption of this approach is that no failure or yarn slippage occurs so that the crossover points deform in an affine manner with the continuum.

We have used this approach to develop a model for the quasi-static, in-plane behavior of a plain weave ballistic fabric, Kevlar® S706. We based this model on a geometry similar to that proposed by Kawabata (1973), but with additional "contact" trusses that allow the geometry to capture locking. The model includes elastic yarn stretching, bending, cross-sectional compression at the crossover points, locking, and both elastic and dissipative relative yarn rotation.

We have implemented this model into ABAQUS/Standard and used it to predict the outcome of uniaxial tensile tests on fabric strips loaded in the warp, weft, and bias directions. In all three cases, the model accurately predicted the experimentally observed deformations and the macroscopic load–extension responses using independently measured properties. We also showed that the model can predict the response of the fabric at the mesostructural level, and that this behavior can be used to predict the onset of failure.

We are conducting further research on three different aspects of fabric mechanical behavior: we are developing a more refined model capable of capturing slippage and other failure mechanisms; we are expanding the model to a three dimensional shell implementation to capture out-of-plane deformations of the fabric; and we are developing improved testing capabilities, including biaxial tension tests, to better measure individual yarn properties, study yarn interactions, better validate the existing model, and investigate and quantify phenomena such as yarn slip, out-of-plane deformations, and high rate deformations. Other potential avenues of further research include the implementation of more complex fabric geometries, the investigation and modeling of contact between multiple layers of woven materials, and the extension of our model to other woven fabrics for applications in a variety of industries, particularly to "structural fabrics" (such as air beams or parachutes) and to woven fabric composites.

Acknowledgement

The authors would like to thank Dr. James Singletary of DuPont and Dr. Phil Cunniff of the US Army Soldier Systems Center, Natick, for information about ballistic fabrics and ballistic impact behavior. Kevlar® samples were provided by DuPont.

This research was supported by the US Army through the Institute for Soldier Nanotechnologies, under Contract DAAD-19-02-D-0002 with the US Army Research Office. The content does not necessarily reflect the position of the Government, and no official endorsement should be inferred.

References

Baseau, E., 2003. Finite deformation of elastic–plastic filamentary networks. International Journal of Nonlinear Mechanics 38, 1473–1479.

Boisse, P., Borr, M., Buet, K., Cherouat, A., 1997. Finite element simulations of textile composite forming including the biaxial fabric behavior. Composites Part B 28B, 453–464.

Boisse, P., Buet, K., Gasser, A., Launay, J., 2001. Meso/macro-mechanical behavior of textile reinforcements for thin composites. Composites Science and Technology 61 (3), 395–401.

Ben Boubaker, B., Haussy, B., Ganghoffer, J.F., 2002. Discrete models of woven structures: stability and draping analysis. C.R. Mecanique 330, 871–877.

Breen, D.E., House, D.H., Wozny, M.J., 1994. A particle-based model for simulating the draping behavior of woven cloth. Textile Research Journal 64 (11), 663–685.

Chen, B., Lang, E.J., Chou, T., 2001. Experimental and theoretical studies of fabric compaction behavior in resin transfer modeling. Materials Science and Engineering A317, 188–196.

Cunniff, P.M., 1992. An analysis of the system effects in woven fabrics under ballistic impact. Textile Research Journal 62 (9), 495–509.

Cherouat, A., Billouet, J.L., 2001. Mechanical and numerical modelling of composite manufacturing processes: deep-drawing and laying-up of thin pre-imprognated woven fabrics. Journal of Materials Processing Technology 118, 460–471.

Gommers, B., Verpoest, I., Van Houtte, P., 1996. Modelling the elastic properties of knitted-fabric-reinforced composites. Composites Science and Technology 56, 685–694.

Hearle, J.W.S., Grosberg, P., Backer, S., 1969. Structural Mechanics of Fibers, Yarns, and Fabrics. Wiley-Interscience, New York.

Kato, S., Yoshiro, T., Minami, H., 1999. Formulation of constitutive equations for fabric membranes based on the concept of fabric lattice model. Engineering Structures 21, 691–708.

Kawabata, S., Niwa, M., Kawai, H., 1973a. The finite deformation theory of plain weave fabrics. Part I: The biaxial deformation theory. Journal of Textile Instiute 64 (1), 21–46.

Kawabata, S., Niwa, M., Kawai, H., 1973b. The finite deformation theory of plain weave fabrics. Part II: The uniaxial deformation theory. Journal of Textile Institute 64 (2), 47–61.

Kawabata, S., Niwa, M., Kawai, H., 1973c. The finite deformation theory of plain weave fabrics. Part III: The shear deformation theory. Journal of Textile Institute 64 (2), 62–85.

MacGlockton, M.A., Cox, B.N., McMeeking, R.M., 2003. A binary model of textile composites: III. Hight failure strain and work of fracture in 3D weaves. Journal of the Mechanics of Physics and Solids 51, 1573–1600.

McGuinness, G.B., O'Bradaigh, C.M., 1997. Development of rheological models for forming flows and picture-frame shear testing of fabric reinforced thermoplastic sheets. Journal of Non-Newtonian Fluid Mechanics 73, 1–28.

Mohammed, U., Lekakou, C., Dong, L., Bader, M.G., 2000. Shear Deformation and Micromechanics of Woven Fabrics. Composites Part A 31, 299–308.

Ng, S., Tse, P., Lau, K., 1998. Numerical and experimental determination of the in-plane elastic properties of 2/2 Twill weave fabric composites. Composites Part B 29B, 735–744.

Press, W.H., Teukolsky, S.A., Vettering, W.T., Flannery, B.P., 1992. Numerical Recipes in FORTRAN: The Art of Scientific Computing, second ed. Cambridge University Press, Cambridge.

Peng, X.Q., Cao, J., Chen, J., Xue, P., Lussier, D.S., Lui, L., 2004. Experimental and numerical analysis on normalization of picture frame tests for composite materials. Composites Science and Technology 64, 11–21.

Peirce, F.T., 1937. The geometry of cloth structure. Journal of Textile Institute 28 (3), T45–T96.

Rattensperger, H., Eberhardsteiner, J., Mang, H.A., 2003. Numerical investigation of high pressure hydraulic hoses with steel wire braid. In: IUTAM Symposium on Computational Mechanics of Solid Materials at Large Strains. pp. 407–416.

Raun, X., Chou, T., 1995. Experimental and theoretical studies of the elastic behavior of knitted fabric composites. Composites Science and Technology 56, 1391–1403.

Realff, M.L., 1992. Mechanical properties of fabrics woven from yarns produced by different spinning technologies. Ph.D. Thesis, Massachusetts Institute of Technology.

Realff, M.L., Boyce, M.C., Backer, S., 1997. A micromechanical model of the tensile behavior of woven fabric. Textile Research Journal 67 (6), 445–459.

Reese, S., 2003. Anisotropic elastoplastic material behavior in fabric structures. In: IUTAM Symposium on Computational Mechanics of Solid Materials at Large Strains. pp. 201–210.

Roylance, D., Chammas, P., Ting, J., Chi, H., Scott, B., 1995. Numerical modeling of fabric impact. In: Proceedings of the National Meeting of the ASME.

Sagar, T.V., Potluri, P., Hearle, J.W.S., 2003. Mesoscale modelling of interlaced fibre assemblies using energy method. Computational Material Science 28, 49–62.

Shim, V.P.W., Tan, V.B.C., Tay, T.E., 1995. Modelling deformation and damage characteristics of woven fabric under small projectile impact. International Journal of Impact Engineering 16 (4), 585–605.

Shim, V.P.W., Lim, C.T., Foo, K.J., 2001. Dynamic mechanical properties of fabric armour. International Journal of Impact Engineering 25, 1–15.

Shockey, D.A., Elrich, D.C., Simons, J.W., 1999a. Improved Barriers to Turbine Engine Fragments: Interim Report I. DOT/FAA AR-99/8,I.

Shockey, D.A., Elrich, D.C., Simons, J.W., 1999b. Improved Barriers to Turbine Engine Fragments: Interim Report II. DOT/FAA AR-99/8,II.

Shockey, D.A., Elrich, D.C., Simons, J.W., 2001. Improved Barriers to Turbine Engine Fragments: Interim Report III. DOT/FAA AR-99/8,III.

Shockey, D.A., Elrich, D.C., Simons, J.W., 2002a. Improved Barriers to Turbine Engine Fragments: Interim Report IV. DOT/FAA AR-99/8,IV.

Shockey, D.A., Elrich, D.C., Simons, J.W., 2002b. Improved Barriers to Turbine Engine Fragments: Final Annual Report. DOT/FAA AR-99/8,V.

Steigmann, D.J., 1992. Equilibrium of prestressed networks. IMA Journal of Applied Mathematics 48 (2), 195–215.

Tanov, R.R., Brueggert, M., 2003. Finite element modelling of non-orthogonal loosely woven fabrics in advanced occupant restraint systems. Finite Elements in Analysis and Design 39, 357–367.

Warren, W., 1992. The large deformation elastic response of woven kevlar fabric. Polymer Composites 13 (4), 278–284.

Xue, P., Peng, X., Cao, J., 2003. A non-orthogonal constitutive model for characterizing woven composites. Composites Part A 34, 183–193.